Medical Engineering and Physics 68 (2019) 35–45

Contents lists available at ScienceDirect

Medical Engineering and Physics

journal homepage: www.elsevier.com/locate/medengphy

Twente Spine Model: A thorough investigation of the spinal loads in a complete and coherent musculoskeletal model of the human spine

Riza Bayoglu[a,*], Pavel E. Galibarov[b], Nico Verdonschot[a,c], Bart Koopman[a], Jasper Homminga[a]

[a] Department of Biomechanical Engineering, University of Twente, P.O. Box 217, AE Enschede 7500, the Netherlands
[b] AnyBody Technology A/S, Aalborg, Denmark
[c] Radboud University Medical Center, Radboud Institute for Health Sciences, Orthopaedic Research Laboratory, Nijmegen, the Netherlands

ARTICLE INFO

Article history:
Received 27 November 2018
Revised 12 March 2019
Accepted 30 March 2019

Keywords:
Spinal loads
Musculoskeletal model
Intradiscal pressure
Subject-specific
AnyBody

ABSTRACT

Although *in vivo* spinal loads have been previously measured, existing data are limited to certain lumbar and thoracic levels. A detailed investigation of spinal loads would assist with injury prevention and implant design but is unavailable. In this study, we developed a complete and coherent musculoskeletal model of the entire human spine and studied the intervertebral disc compression forces for physiological movements on three anatomical planes. This model incorporates the individual vertebrae at the cervical, thoracic, and lumbar regions, a flexible ribcage, and complete muscle anatomy. Intradiscal pressures were estimated from predicted compressive forces, and these were generally in close agreement with previously measured data. We found that compressive forces at the trunk discs increased during trunk lateral bending and axial rotation of the trunk. During flexion, compressive forces increased in the thoracolumbar and lumbar regions and slightly decreased at the middle thoracic discs. In extension, the forces generally decreased at the thoracolumbar and lumbar discs whereas they slightly increased at the upper and middle thoracic discs. Furthermore, similar to a previous biomechanical model of the cervical spine, our model predicted increased compression forces in neck flexion, lateral bending, and axial rotation, and decreased forces in neck extension.

1. Introduction

Spinal loads have been previously quantified mostly through intervertebral disc pressures or instrumented implants. Several authors have measured *in vivo* pressures at the lumbar and thoracic discs [1–6]. Differently, resultant forces and moments on lumbar telemetered implants were measured [7]. Although detailed knowledge of spinal loads is available, it is limited to certain levels in the lumbar and thoracic regions due to ethical issues. Also, this data has been valuable for estimating the compressive forces at the intervertebral discs but less so for other forces such as shear forces at the discs or muscle forces. A comprehensive assessment of spinal loads would assist with injury prevention and implant design but is yet unavailable.

Several researchers have developed validated models to explore the nature of the loads within the spine [8–14]. These models have evolved in complexity for representing generic or subject-specific musculoskeletal systems. Compared to generic models, subject-specific models offer more realistic representations of the skeletal and muscular anatomy [15]. The majority of these models included only a certain region of the spine and assumed a single, lumped, rigid body representation of the thorax or neck. The effects of modeling the thorax this way instead of a flexible structure when estimating the lumbar loads were previously studied for flexion [16]. They found moderately lower compressive disc forces but remarkably altered muscle forces. It remains unclear how such modeling approaches would affect force predictions when other movements are investigated. The majority of the previous models have relied on anatomical illustrations for defining muscle lines-of-action and lacked deeper spinal muscles which function as joint stabilizers. Recent studies developed methods for implementing moment arms and cross-sectional areas of major trunk muscles from medical images [12]. Obtaining muscle origins and insertions at the bones precisely is still difficult with current imaging modalities particularly for smaller and deeper muscles [17]. Furthermore, muscle parameters that are needed and influential in the model (physiological cross-sectional area (PCSA) for example, [18]) can not be reliably determined from two-dimensional medical

* Corresponding author.
E-mail address: r.bayoglu@hotmail.com (R. Bayoglu).

https://doi.org/10.1016/j.medengphy.2019.03.015
1350-4533/

imaging [17,19]. In essence, there is also a need for a complete and coherent musculoskeletal model of the entire human spine, which is likely to yield realistic spinal loads [15].

Recently we published a musculoskeletal dataset which was measured from one single human body [20,21]. In this dataset, the coordinates of muscle attachments, architectural parameters of 321 muscle-tendon elements, and the spinal geometry were reported. Furthermore, new data were obtained for several muscles in the thoracic and lumbar regions. The objective of this study is now to investigate the compressive forces at the intervertebral discs throughout the spine during basic trunk and neck movements. For this, we developed and used a complete and coherent musculoskeletal model of the entire human spine (based on the previously published dataset) and validated it by comparing calculated spinal loads to *in vivo* measurements. Subsequently, we used this model to determine the spinal loads at every spinal level, which until now could not be determined. This model represents a subject-specific musculoskeletal system and has several particular features, such as incorporation of the individual vertebrae at the cervical, thoracic, and lumbar regions, flexible ribcage, and comprehensive muscular anatomy.

2. Materials and methods

2.1. Development of the model

We developed a musculoskeletal model for the entire human spine in AnyBody Modeling System. This model was based on a coherent anatomical dataset measured from one embalmed cadaver (male, 79 years-old, height: 154 cm, mass: 51 kg) [20,21]. In this model, the bones were idealized as rigid body segments and the muscle-tendon elements as force actuators. The model included 60 segments (vertebrae, ribs, skull, sternum, hyoid, thyrohyoid, clavicles, scapulas, humeri, sacrum, and pelvis) and had 193 DoF (Fig. 1). The lumped masses and the centers-of-mass (CoM) of the body segments were defined based on previous reports [13,22–24]. The hyoid, thyrohyoid, clavicle, scapula, and the humerus segments were included without mass properties as these only functioned as attachment sites for muscles that play a role in lateral bending and axial rotation. Our model does not explicitly incorporate the lower extremity and the shoulder-arm complex nor the body segments and muscles located in these extremities. The arms and other segments are present for further modeling. External forces and moments were applied at the third thoracic vertebrae to model the loads that would be exerted by the shoulder-arm complex [25]. We set the mass moments-of-inertia for all the segments to zero based on the fact that their rotational velocities and accelerations are negligible during basic trunk movements [8].

We utilized previously reconstructed stereolithography (STL) files of the bones [20,21]. First, spinal geometry was made left-right symmetrical. For this, we established a local reference frame for each vertebra and mirrored its right side in the local sagittal plane [26] in Solidworks 2016 (Fig. 1). Similarly, the other bones in the skeletal system also were made left-right symmetrical. Next, the positions and the orientations of the individual segments were adjusted to reconstruct the spinal curvature at the supine position. Finally, muscle attachment sites reported in the global reference frame were expressed in corresponding vertebral frames.

Our model relied on inverse dynamics principles for predicting muscle activations where an optimization function was employed. Similar to previous models [12,13], a third degree, polynomial muscle recruitment criterion was implemented [27].

2.1.1. Muscular anatomy

In total, 351 muscle-tendon elements (per body side) were included for 49 muscles. The isometric muscle strength was calculated by multiplying its PCSA by the specific muscle tension (100 N/cm^2). Because the data for the intercostales and the levatores costarum longi muscles along the entire ribcage was lacking in the original dataset, we introduced additional elements for these muscles at the missing levels. The morphological parameters for these elements were taken as the averages of the measured data. We also incorporated the abdominal muscle implementation from the human body model of the AnyBody Managed Model Repository. The changes in the length of the transversus abdominis muscle elements and the abdominal volume resulted in a change of intra-abdominal pressure, hence force in these muscles. All the muscles included in this study are listed in Table 1.

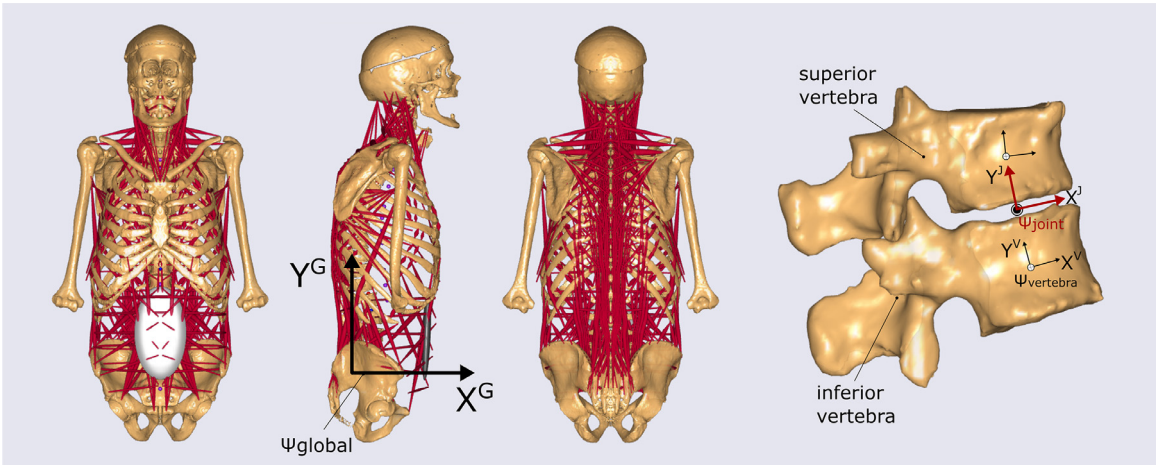

Fig. 1. The musculoskeletal model developed in this study, bones are displayed in beige and muscle-tendon elements in red. The reference frame shown in the sagittal view is the global reference frame (ψ_{global}). The vertebral ($\psi_{vertebra}$) and intervertebral disc joint reference frames (ψ_{joint}) are illustrated for one motion segment. The origin of the vertebral reference frame is located at the centroid of the vertebral body, the *y*-axis passes through the geometric centers of the inferior and superior end-plates, and the *z*-axis is parallel to the line connecting similar landmarks on the left and right pedicles (orthogonal to the sagittal plane). The orientation of the intervertebral joint reference frame is defined as the average of its corresponding superior and inferior vertebra reference frame. The invertebral disc inclinations were calculated as the average angles of the superior and inferior vertebrae on the sagittal plane. The intervertebral compression force is calculated along the *y*-axis of the joint reference frame (perpendicular to the disc inclined plane) while shear is the force component on the *xz* plane (parallel to the disc inclined plane).

Table 1
Muscles included in the model.

Region	Muscle
Cervical spine	Iliocostalis cervicis, Levator scapulae, Longissimus capitis, Longissimus cervicis Longus capitis, Obliquus capitis inferior, Obliquus capitis superior, Omohyoid Rectus capitis anterior, Rectus capitis lateralis, Rectus capitis posterior major Rectus capitis posterior minor, Scalenus anterior, Scalenus medius, Scalenus posterior Semispinalis capitis, Semispinalis cervicis, Splenius capitis, Splenius cervicis Sternocleidomastoid, Sternohyoid, Sternothyroid, Thyrohyoid
Thoracic spine	Iliocostalis thoracis, Rhomboideus major, Rhomboideus minor, Rotatores Semispinalis thoracis, Serratus anterior, Serratus posterior superior, Spinalis thoracis Subclavious, Trapezius
Ribcage	Intercostales externi, Intercostales interni, Levatores costarum Subcostales, Transversus thoracis
Lumbar spine	Iliocostalis lumborum, Latissimus dorsi, Longissimus thoracis, Multifidus Obliquus externus abdominis, Obliquus internus abdominis, Psoas major Quadratus lumborum, Rectus abdominis, Serratus posterior inferior Transversus abdominis

Table 2
The stiffness data adapted from the literature [53,54].

Joints	Flexion [Nm/deg]	Extension [Nm/deg]	Lateral bending [Nm/deg]	Axial rotation [Nm/deg]	Tension [kN/m]	Compression [kN/m]	Shear [kN/m]
Intervertebral							
C0/C1	0.04	0.02	0.09	0.06	fixed	fixed	fixed
C1/C2	0.06	0.05	0.09	0.07	fixed	fixed	fixed
C2–T1	0.43	0.73	0.68	1.16	fixed	fixed	fixed
T1–T12	2.65	3.25	2.27	2.60	fixed	fixed	fixed
T12–S1	1.80	2.60	2.30	6.90	fixed	fixed	fixed
Costovertebral	fixed	fixed	fixed	fixed	4.9	49	fixed
Costotransverse	0.12	0.12	0.12	0.17	4.9	49	123

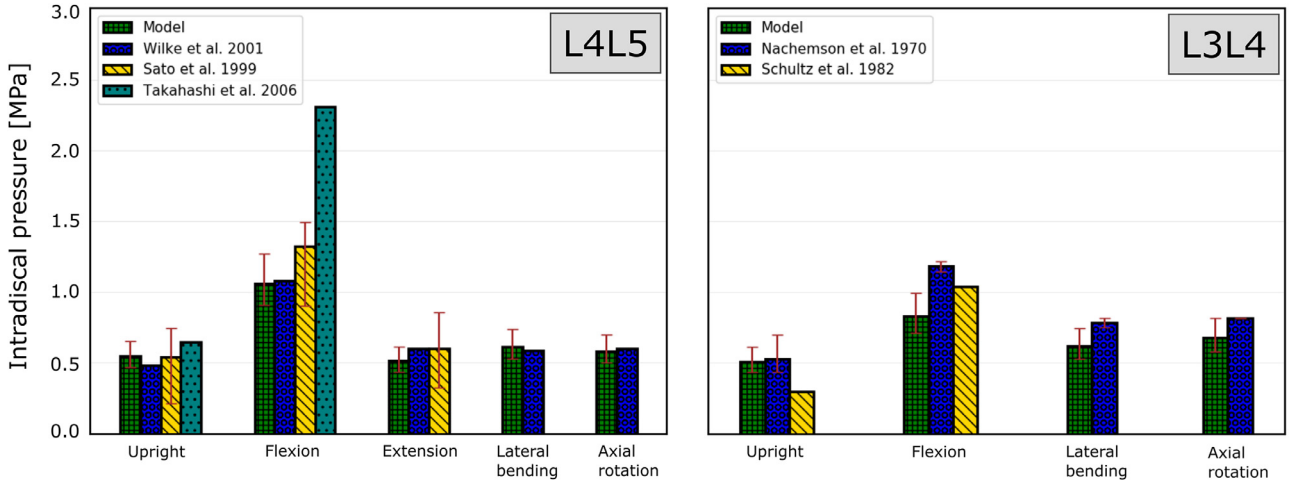

Fig. 2. Intradiscal pressures at the L4/L5 and L3/L4 discs. The error bars placed over the model's predictions represent the range due using the minimum and maximum correction factors [36] whereas those placed over the experimental data show intersubject variance.

2.2. Joints

The intervertebral articulations were modeled as spherical joints. The locations of lumbar and cervical intervertebral joints were based on previous reports [28,29]. In the thoracic spine, the geometric centers of the intervertebral discs were used. The costosternal articulations between the costal cartilages and the sternum were defined as six DoF joints. The costotransverse and the costovertebral joints were simplified as single-compound revolute joints which allowed rotation about the ribs' cervical axes [13,30]. We defined the locations and reference frame axes of the aforementioned joints in line with previous studies [31–33]. Sternoclavicular, acromioclavicular, glenohumeral, and the articulations of the hyoid and the thyroid bones with the C3 and C4 vertebrae, respectively, were modeled as six DoF joints. No movement was prescribed at these joints implying that they were rigidly connected to the segments they articulated with.

The elastic behavior of the intervertebral joints was modeled as a lumped stiffness induced by the ligaments, discs, and the facet joints using linear torsion springs in three directions. In addition, the tension/compression stiffnesses for the costovertebral articulations and the tension/compression, shear, and the bending

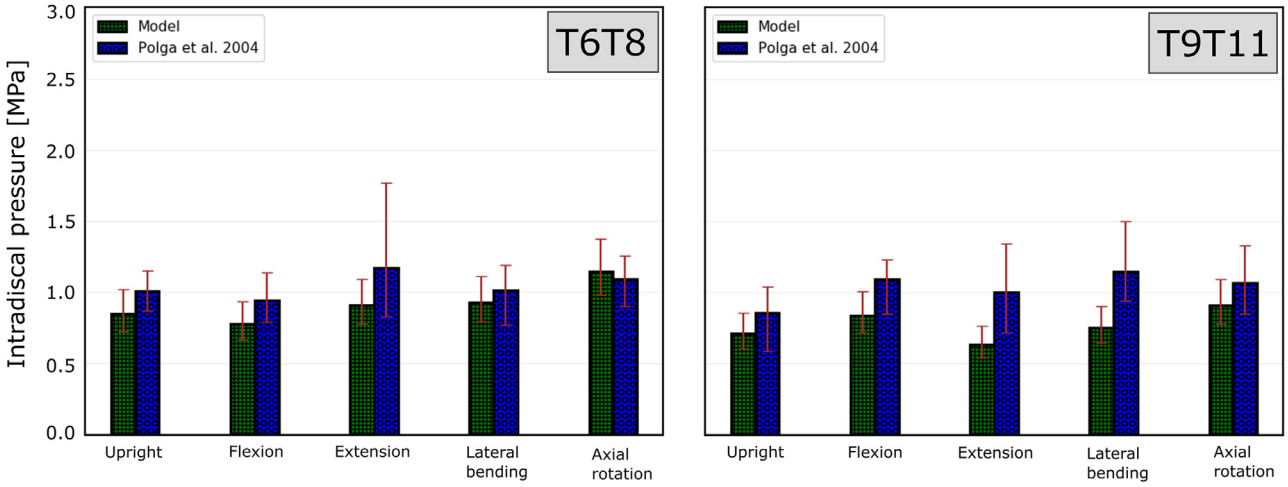

Fig. 3. Intradiscal pressures at the middle (T6–T8) and lower T9–T11 thoracic discs. Our estimates were computed as the averages of the pressures calculated at the T6/T7 & T7/T8, and T9/T10 & T10/T11 discs.

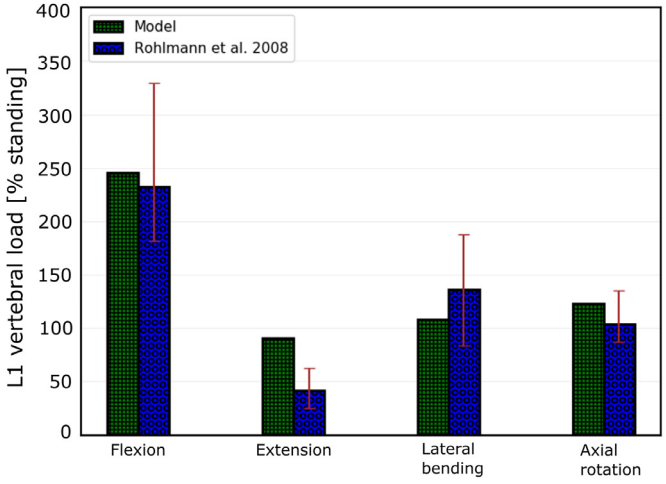

Fig. 4. Resultant forces (normalized to standing) at the L1 vertebra. These forces were calculated as the average of the loads at the T12/L1 and L1/L2 disc joints. The error bars indicate the variance measured in two patients [7].

Table 3
Intervertebral disc cross-sectional areas quantified from the CT images.

Disc	Area (mm^2)
T6/T7	667
T7/T8	727
T9/T10	852
T10/T11	954
L3/L4	1367
L4/L5	1398

stiffnesses for the costotransverse articulations were defined using the stiffness data reported in previous studies (Table 2).

Soft constraints were applied for prescribing the movement at the compound-costotransverse and costovertebral joints and the costosternal joints. These constraints allowed minimal deviation from the idealized joints by minimizing the total elastic energy of deformation and determined the movement at these joints. This approach facilitated defining the otherwise mechanically

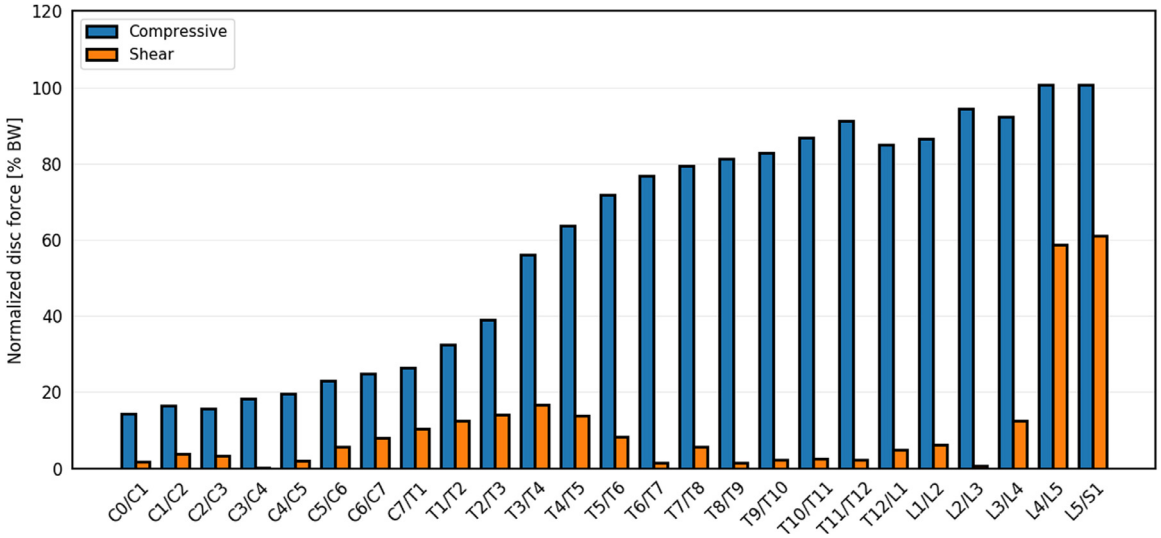

Fig. 5. Compressive and anterior-posterior shear forces at the intervertebral disc joints during standing upright. The forces were expressed as percentages of the total body weight (BW) of the cadaver.

Table 4
Predicted forces (N) in major trunk muscles compared to previous studies.

	Erector spinae				Latissimus dorsi			Rectus abdominis			Obliquus internus abdominis			Obliquus externus abdominis		
	Present	S[a]	K[b]	H[c]	Present	S[a]	H[c]	Present	S[a]	K[b]	Present	S[a]	K[b]	H[c]	Present	S[a]	K[b]	H[c]
Upright	144	0	26	27	46	100	27	0	0	0	25	0	0	57	18	4	0	97	16
Flexion	276	290	314	264	21	240	11	0	0	6	0	17	0	4	37	37	0	0	18
Extension	42	0	36	15	65	0	0	0	220	81	340	4	0	16	23	9	0	0	4
Lateral bending	146	70	36	63	46	200	86	0	0	0	35	15	160	97	100	18	260	120	63
Axial rotation	148	90	91	34	97	180	46	0	0	0	50	47	129	16	29	39	150	34	29

References:
[a] Schultz et al. (1982) [2]
[b] Khurelbaatar et al. (2015) [14]
[c] Han et al. (2012) [44]

Table 5
Intervertebral disc inclinations on the sagittal plane.

Disc	Angle (°)
C2/C3	0.0
C3/C4	−14.3
C4/C5	−23.6
C5/C6	−27.0
C6/C7	−30.3
C7/T1	−36.0
T1/T2	−37.3
T2/T3	−37.2
T3/T4	−34.9
T4/T5	−31.2
T5/T6	−22.0
T6/T7	−10.9
T7/T8	−6.4
T8/T9	−0.2
T9/T10	3.6
T10/T11	5.3
T11/T12	9.4
T12/L1	11.6
L1/L2	9.0
L2/L3	1.6
L3/L4	−12.2
L4/L5	−35.6
L5/S1	−44.3

over-constrained nature of the costosternal joints in a kinematically determinant way [34].

2.3. Comparison with in vivo intradiscal pressures

We compared the model's prediction of spinal loading with the previous *in vivo* studies [1–6]. For this, the same tasks investigated in these studies were simulated, and the estimated intradiscal pressures were compared. We only included experimental data measured from healthy discs. The intradiscal pressures (in MPa) were calculated according to Eq. (1):

$$IDP_{model} = \frac{F_C}{DA \times CF} \tag{1}$$

where F_C represents the predicted compressive force (in N) at the intervertebral joint (Fig. 1), DA represents the disc cross-sectional area (in mm^2), and CF represents a correction factor needed when calculating compression forces from intradiscal pressures [35]. Dreischarf et al. 2013 reported this correction factor to be 0.66 ± 0.11. Therefore, we calculated the intradiscal pressures by using three values for the correction factor ($CF_{\min} = 0.55$, $CF_{mean} = 0.66$, and $CF_{\max} = 0.77$). For comparison purposes, the median values were plotted, and the error bars placed over the model's estimates represent the range due using different correction factors ($CF_{\min}$ and $CF_{\max}$) (Figs. 2 and 3). The pressure magnitudes measured at the L3/L4 disc were corrected by subtracting 0.25 MPa as suggested by Nachemson and Elfstrom [1,36]. Intervertebral disc cross-sectional areas were quantified from the medical images and are given in Table 3.

2.4. Simulated tasks

We simulated several quasi-static tasks with the model. Each task started from the standing upright position and finished when the specified maneuver (such as trunk flexion) was achieved. We performed these simulations for trunk and neck regions separately (referred to as trunk and neck tasks). For neck tasks, we distributed the total motion over the intervertebral joints between the skull and T1 segments (hence no trunk motion). Similarly, for the trunk tasks, we only specified the motion between T1

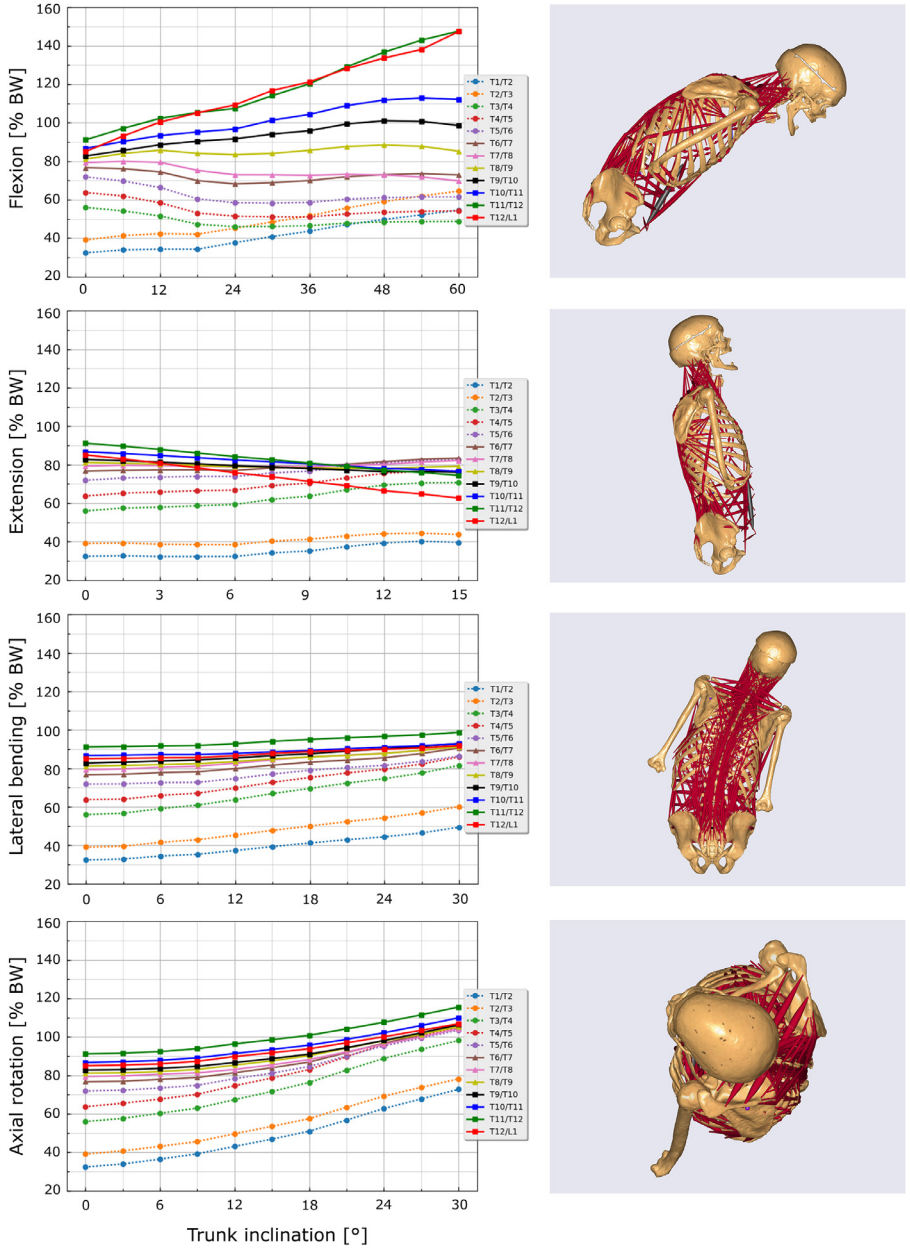

Fig. 6. Disc compressive forces in the thoracic spine as functions of trunk inclination. The end postures in each task are shown next to the plots.

and pelvis segments (no neck motion) and partitioned the motion accordingly. The partitioning of the motion across each intervertebral joint took place according to the spinal rhythm matrices derived from previous reports [37–42]. Furthermore, the total trunk motion was distributed between the pelvis and thoracic and lumbar regions of the spine. The amount of pelvic rotation in flexion and extension was calculated by using the lumbopelvic ratios reported by Tafazzol et al. [43]. 20%, 73%, and 83% thoracic motion (out of the total rotation in the lumbar and the thoracic intervertebral joints) was used for the trunk flexion, extension, lateral bending, and axial rotation tasks, respectively. For the trunk tasks, we simulated standing upright, flexion (60°), extension (15°), lateral bending (30°), and axial rotation (30°) maneuvers. For the neck tasks, standing upright, flexion (45°), extension (15°), lateral bending (20°), and axial rotation (20°) were simulated. All the simulations were batch-processed and post-processed in Python 3.6 environment using AnyPyTools library.

3. Results

3.1. Comparison of spinal loading with in vivo measurements

Calculated intradiscal pressures at the lumbar region (L4/L5 and L3/L4 discs in Fig. 2) were highly correlated to previous experimental measurements [1–5] ($R = 0.91$ and RMSE = 0.16). However, the model slightly underpredicted the compressive loading at the L3/L4 disc for certain postures. When the two levels were analyzed separately, the following correspondences were found: L4/L5 ($R = 0.95$ and RMSE = 0.11) and L3/L4 ($R = 0.95$ and RMSE = 0.21). The thoracic disc pressures (T6–T8 and T9–T11 discs in Fig. 3) predicted by the model were generally within the range previously reported [6], though a good correlation was lacking ($R = 0.45$ and RMSE = 0.23). The model predicted the trends (the pressure change compared to upright position) qualitatively well except for the lower thoracic discs in extension. Furthermore, the model captured the relative pressure levels between the middle and lower

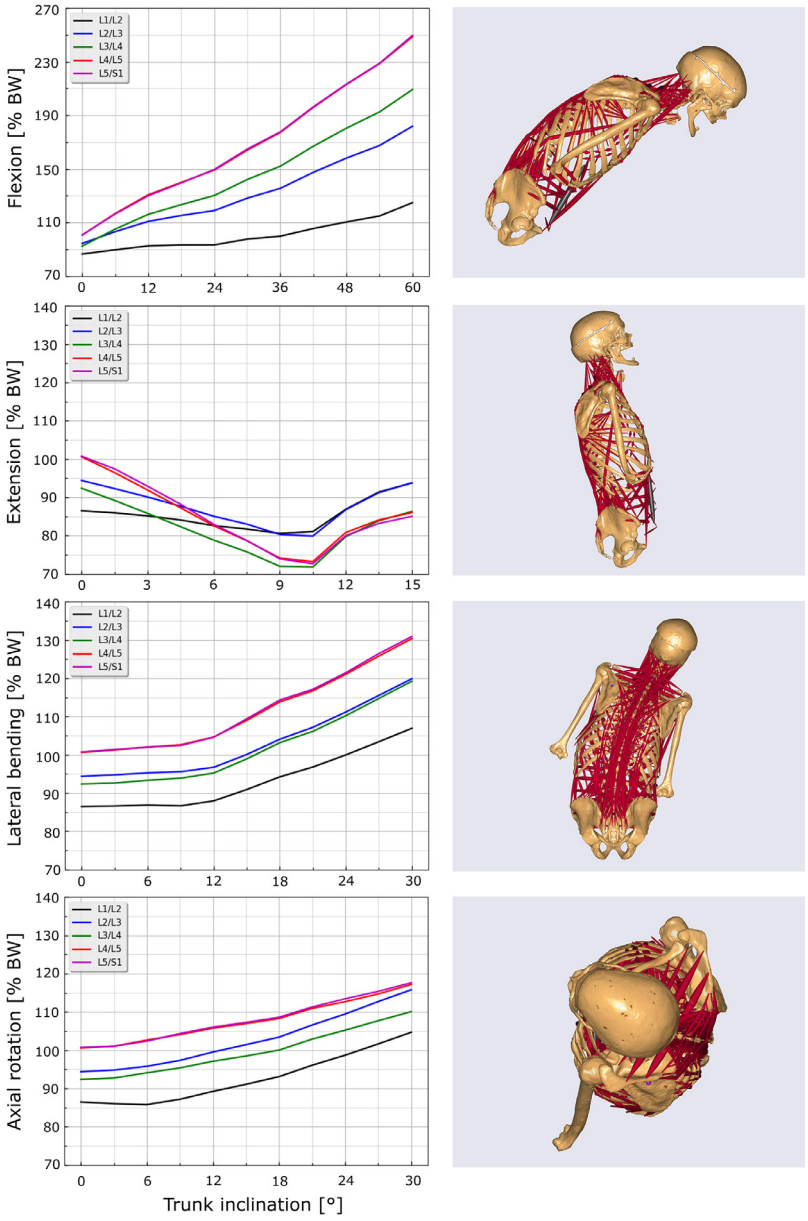

Fig. 7. Disc compressive forces in the lumbar spine as functions of trunk inclination. The end postures in each task are shown next to the plots.

thoracic discs well except in lateral bending where our model predicted higher pressures at the middle thoracic discs than the lower levels. Moreover, the model predicted the trends well for the upright posture that the pressure levels (median values) from the highest to the lowest (similar to previous experiments) were as follows: T6–T8, T9–T11, L4/L5, and L3/L4. Further, we compared normalized resultant loads (as the percentage of the load at the upright standing) predicted by the model with the loads quantified from the instrumented devices implanted at the L1 vertebrae in Fig. 4. The model's estimates were within the measured range except in extension where the model overpredicted the normalized loads.

3.2. Comparison of muscle function with previous studies

Muscle forces and their activation patterns computed by the model were compared to previous modeling and experimental studies in Table 4. Although force magnitudes differed, in general, our model predicted similar activation trends to previous experimental and computational studies [2,14,44]. For example, erector spinae muscle group was prevalent in flexion and also played a role in lateral bending and axial rotation of the trunk. Latissimus dorsi was active during all the movements and was dominant in axial rotation. Similar to EMG measurements, except for extension, rectus abdominis was inactive. Obliquus internus abdominis and obliquus externus abdominis muscles followed similar patterns, and they were mainly active during trunk flexion, lateral bending, and axial rotation.

3.3. Intervertebral disc joint forces

3.3.1. Compressive and shear forces at the standing upright position

Compressive and anterior-posterior shear forces predicted at the intervertebral disc joints during standing were expressed as percentages of the total body weight (BW) and are shown in Fig. 5. The smallest and the largest compressive forces were found at

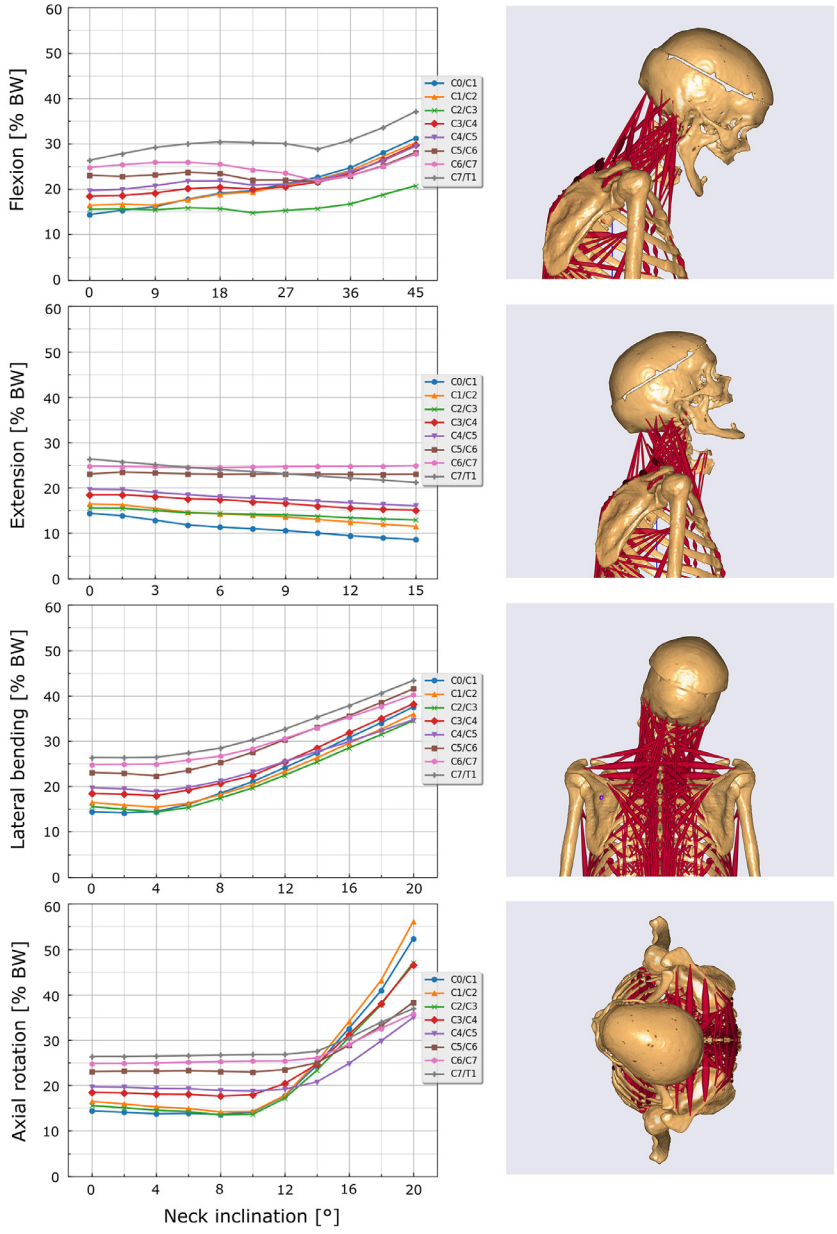

Fig. 8. Disc compressive forces in the cervical spine as functions of neck inclination. The end postures in each task are shown next to the plots.

the C0/C1 (14%) and L5/S1 (101%) joints, respectively. The compressive forces increased from cervical to lumbar, and there were some fluctuations at the thoracolumbar junction and middle lumbar levels. The median values for the cervical (C0–T1), thoracic (T1–L1), and lumbar (L1–S1) regions were 20%, 70%, and 95% of body weight, respectively.

Shear forces were remarkably lower than the compressive forces throughout the spine, and they were relatively higher at the upper thoracic and lower lumbar levels. The lowest and the highest shear forces were found at the C3/C4 (0.2%) and L5/S1 (61%) joints, respectively. Regional medians were as follows: cervical (4%), thoracic (7%), and lumbar (28%). The correlation analysis between the disc inclinations (Table 5) and shear forces did not reveal a significant relation ($R = 0.64$) across all discs. However, when the three regions were analyzed separately, we found good to strong relations between disc inclination and shear force: cervical ($R = 0.69$), thoracic ($R = 0.95$), and lumbar ($R = 0.99$).

3.3.2. Compressive forces during trunk tasks

We present the model's compressive forces at the thoracic and lumbar discs during the motion for the trunk (Figs. 6 and 7): standing upright, flexion, extension, lateral bending, and axial rotation. The forces were computed as percentages of the total body weight of the cadaver.

In general, flexion caused the largest spinal loads at the lumbar and thoracic discs at the final positions among all the maneuvers. When the same trunk rotations were considered (30° flexion, lateral bending, and axial rotation), axial rotation generally induced higher loading at the thoracic discs, whereas forward flexion induced higher loads in the lumbar discs. The disc forces mainly increased with increasing trunk motion except in extension where they decreased at the lower thoracic and lumbar discs. Furthermore, in general, the forces increased caudally.

In forward flexion, the compressive forces at the upper and lower thoracic discs as well as the lumbar discs gradually increased

whereas they slightly decreased at the middle thoracic discs with increased trunk inclination. At 60° trunk flexion, the highest and lowest forces were noted for the L5/S1 (250%) and T3/T4 (49%) joints, respectively.

In extension, the forces in the thoracolumbar and lumbar regions slightly decreased until around 10°, after which they gradually increased. The forces at the upper and middle thoracic joints slightly increased, and the lower thoracic discs had smaller compression (10–23% decrease) compared to upright posture. At the end of the maneuver, the L2/L3 disc had the highest compression (94%), and the T1/T2 disc had the lowest (40%).

Lateral bending increased the compression at all the discs gradually and almost linearly, around 6 to 25% rise at the thoracic discs and 20 to 30% rise at the lumbar discs. The highest and lowest forces were predicted for the L5/S1 (131%) and T1/T2 (49%) joints, respectively.

Similar to lateral bending, axial rotation increased the disc compressions almost linearly at all the joints. Compared to lateral bending, axial rotation led to relatively higher increases in the thoracic region yet smaller in the lumbar region. We found the largest and smallest forces as 118% at the L5/S1 joint and 73% at the T1/T2 joint, respectively.

3.3.3. Compressive forces during neck tasks

The compressive forces at the cervical discs (Fig 8) were much lower than those of the lumbar and thoracic discs. In general, the forces increased in flexion, lateral bending, and axial rotation but decreased in extension. Lateral bending induced the largest forces at the lower discs (43% at C7/T1) whereas axial rotation did at the upper discs (56% at C1/C2).

In flexion, the highest and lowest forces were noted at the C7/T1 (37%) and C2/C3 (21%) joints, respectively. Compared to the neutral position, the force increases ranged from 3% (C6/C7) to 17% (C0/C1).

In extension, the compressions gradually decreased except at the C5/C6 and C6/C7 discs where they almost did not change compared to neutral position. The model predicted the highest and lowest forces at the C6/C7 (25%) and C0/C1 (9%) joints, respectively.

During early lateral bending, the forces did not change much until around 4° but consistently increased afterward at all the joints roughly linearly. The highest and lowest forces were found at the C7/T1 (43%) and C4/C5 (32%) discs.

In axial rotation, the forces first did not change much until around 10–14° but increased rapidly afterward at all the joints. At the final position, the upper joints were loaded the largest. All the joints had significantly higher forces at the end of the maneuver when compared to upright position. The C1/C2 joint had the largest force (56%) and C4/C5 (35%) the smallest.

4. Discussion and conclusion

Accurate characterization of spinal loads is fundamental to understanding normal and pathological spine functioning [45], injury prevention during occupational tasks [10], optimization of surgical interventions, and pre-clinical testing of implants. In the past, spinal loads have been measured through intervertebral disc pressures and telemetered vertebral implants [1–7]. Despite these previous experimental studies, our understanding of the relation between the movement and the spinal loads remains largely unexplored mainly due to technical difficulties in experimentation and the related ethical concerns. Musculoskeletal modeling accommodates great opportunities to study spine biomechanics in depth and to estimate *in vivo* loads.

In this study, we developed a complete and coherent musculoskeletal model of the entire human spine by incorporating the anatomical dataset reported in earlier work [20,21]. When developing this model, skeletal and muscle morphologies were reconstructed from this dataset while segment mass properties, joint definitions, and stiffness properties, and spinal rhythms were implemented based on previous investigations. Since all the muscle and skeletal data were obtained from one single spine, our model essentially represents a subject-specific musculoskeletal system and, unlike generic models, it does not require combining anatomical data from other datasets [15]. This model includes body segments, mechanical joints to mimic their articulations, and muscle groups and can predict spinal loading using an inverse dynamic approach. The inherent redundancy in the musculoskeletal system is solved using an optimization criterion in which muscle activations are computed based on minimization of muscle fatigue. Our model has several particular features, such as the incorporation of individual vertebrae (cervical, thoracic, and lumbar), flexible ribcage, and comprehensive muscular anatomy which included various deeper muscles in the spine. Incorporation of non-rigid cervical and thoracic spines enables more realistic and detailed investigations of the muscle activation patterns and the spinal loads [16]. These features might be particularly important when studying the joints connecting different regions of the spinal column (for example, C7/T1 joint) as the changes in moment arms of the muscles spanning these joints would be better implemented.

We calculated the intradiscal pressures from predicted compressive forces at the disc joints during physiological trunk movements. For this, we simulated several trunk postures similar to previous experiments where *in vivo* pressures at certain lumbar and thoracic discs were measured. Disc pressures estimated by our model at the L4/L5 and L3/L4 levels were overall in good agreement ($R = 0.91$) with the previous data from several investigations [1–5]. For the third lumbar disc, we used the data measured in two different studies [1,2]. These studies reported intradiscal pressures in a broad range (0.3 – 0.7 MPa) and found increases in pressures during trunk flexion. Our model underpredicted the compression at this disc level during flexion and side lateral bending but predicted the increase trends compared to upright position well (Fig. 2). Polga et al. reported the pressures at the middle and lower thoracic discs from six healthy individuals [6]. Polga's data also showed significant variations for all the trunk postures yet relatively higher variations in extension and lateral bending. Nevertheless, the model's estimations were generally within the range reported, and it predicted the change in pressures compared to upright position qualitatively well except for the lower discs during extension (Fig. 3). In addition, the model captured the relative pressures between the middle and lower discs (except in lateral bending) in accordance with the measurements. These variances between the *in vivo* data, as well as the discrepancies in our findings, can perhaps be explained by subject-specific factors such as spinal curvature and rhythm or simplified modeling of the arms as lumped masses [46]. Finally, our estimations at the thoracic and lumbar levels during an upright position were in excellent agreement with the experimental data. We found that the pressures decreased caudally from 0.85 MPa at T6–T8 and 0.71 MPa at T9–T11 to 0.51 MPa at L3/L4 but then increased to 0.55 MPa at L4/L5 disc [36]. In this study, we generally achieved good agreements with the previous *in vivo* measurements at the lumbar and thoracic discs. This demonstrated a preliminary validation of our model and gave us the confidence to study the development of the compression forces at the intervertebral discs during basic activities of daily living. It is important to note that further validation of the model in terms of muscle forces and joint moments under more demanding activities is necessary. This will enable to expand the model's credibility for investigating occupational tasks such as manual materials handling and will be the subject of future research.

During standing, predicted compressive forces (% BW) at all levels (Fig. 5) were consistently higher than those reported in

previous computational models [10,13,14,16,47] but similar to measured data. For example, previous models' estimations at the L4/L5 disc ranged from 52% to 89% BW whereas *in vivo* data (derived from Dreischarf's review paper [36]) indicated huge variations: Wilke et al. [4] (71%–99%), Sato et al. [3] (22%–143%), and Takahashi et al. [5] (54%–75%). We found compression of 101% BW at the L4/L5 disc during standing. For the T9/T10 disc, previous models found ratios ranging from 31% to 77% while data from Polga et al. [6] suggests between ∼33% and ∼81% (estimated from the reported range and disc areas [48]). We found a comparable compressive force of 83% BW at the T9/T10 level. We saw that similar variations existed for the third lumbar and middle thoracic discs and that our estimations fit within the *in vivo* data reported. Furthermore, our predictions of compression forces were closest to those reported from a generic musculoskeletal model of the thoracolumbar spine which assumed a single-lumped rigid body representation of the neck and overpredicted intradiscal pressures at the thoracic discs [13]. Predicted anterior-posterior shear forces during standing (Fig. 5) were also generally higher than those found in the aforementioned models which reported varying shear force distributions at the lumbar spine. Previous models estimated the forces between ∼4% and ∼10% BW at the first lumbar disc compared to the current study (6%) and the experimental measurements ∼10% [7]. This indicated that our prediction of the anterior-posterior shear at the L1/L2 level was in accordance with the previous models and the *in vivo* data. Unfortunately, we are unaware of any experimental data to validate our predictions further at the other levels. The variations between the previous models and our cadaver-based model are possibly due to the differences in the simulated muscle and skeletal anatomy or modeling practices.

Dreischarf et al. [35] elaborated that the compressive forces at the healthy intervertebral discs can be estimated from the intradiscal pressures during all the maneuvers studied in this work except extension. They found increasing facet joint forces, decreasing disc forces and discussed the non-proportionality of the pressure and compression force during extension because the pressure increased *in vivo* [4]. In extension, we found decreasing compression forces at the thoracolumbar discs and slightly increasing forces at the middle thoracic discs with increased trunk inclinations (Fig. 6). At the lumbar discs, the forces descended during early extension but increased later for trunk angles larger than ∼10° (Fig. 7). This increase was caused by saturated activities of deep muscles such as spinalis thoracis, rotatores, and multifidus to balance the external loads around the thoracolumbar joints. Due to this force increase at the L1/L2 joint (although a decrease at the T12/L1 joint), our model, similar to the previous models [12,14,44], overpredicted the normalized loads at the L1 level in extension (Fig. 4). Although the rises at the middle thoracic discs and the drops at the lumbar discs during early extension were in accordance with the *in vivo* data, the decreases at the lower thoracic discs and the increases in the lumbar region were in disagreement [6,7]. These suggest that our predictions for extension might not be very reliable after all and necessitates a further study. In line with the experimental studies [4,6,7], we found increased compressions at all the trunk discs during lateral bending and axial rotation maneuvers. Similarly, our simulations indicated increased compressive forces at the lower thoracic discs and lumbar regions and slightly decreased forces at the middle thoracic discs during trunk flexion. These findings were also in agreement with the *in vivo* measurements and differed from a previous thoracolumbar spine model which reported higher compression forces and thus intradiscal pressures (compared to upright position) at the middle thoracic discs [13].

The predicted compressive forces at the cervical discs were significantly lower than those of the thoracic and lumbar discs (Fig. 8). Due to the lack of *in vivo* data on cervical disc pressures, it was not possible to validate our findings for the cervical levels. But when comparing our model's findings to those of previous models, they give similar results. Snijders et al. [49] found in their cervical biomechanical model that disc forces increased during flexion, reached their minimums in extension, increased in lateral bending, and did not change much until 35° axial rotation but increased fast with further axial rotation. Our findings for the cervical joints were in close agreement with these observations. We found that the disc forces increased significantly after ∼14° in axial rotation instead of 35°. Furthermore, the normalized compressive forces at the neutral position were similar to a previous cervico-thoraco-lumbar spine model [14].

Several limitations affect the data presented in this work. Firstly, our model used a simplified approach for modeling the shoulder-arm complex. This practice facilitated including trunk muscles such as latissimus dorsi and trapezius that played roles during lateral bending and axial rotation. We estimated and applied external forces and moments at the third thoracic vertebrae to model the loads due to these extremities [25]. Thus, our model is not usable for tasks that cause large arm forces. Secondly, we used a simple muscle model where force-length and force-velocity relationships were not considered. For simplicity, we opt to not include them as some muscle parameters such as optimal fiber length and tendon slack length would require further calibrations. Thirdly, the intervertebral disc articulations were simplified as spherical joints which lacked translational DoFs. Recent studies discussed that neglecting translational DoFs and thus assuming fixed locations for joint centers of axial rotation might affect the joint reaction and muscle forces [50,51]. Fourthly, we did not model the facet joints. Earlier studies discussed that the facet joints will cause a decrease in the transmission of forces through the anterior column during extension [12,35]. Fifthly, we did not include spinal ligaments but included their collective rotational stiffnesses linearly in the intervertebral and ribcage joints. The lack of ligaments or simplifying their non-linear mechanical behaviors in the model would change the load sharing patterns between the muscles and thus affect our findings [52]. Sixthly, our cadaver-based model was not scaled to match anthropometric features of the subjects volunteered in the previous *in vivo* measurements of spinal loads. We found it more realistic to compare disc pressures as was done in this study rather than applying complex scaling protocols which were not available. Seventhly, this subject-specific model represents an elderly male with a body height of 154 cm and a mass of 51 kg. Thus, the applicability of the findings presented in this work might be limited when individuals with different anthropometric features and morphologies are studied. Finally, we refer the reader to our previous works where limitations peculiar to the anatomical dataset used in this model were described in detail [20,21].

Conflicts of Interest

Pavel E. Galibarov works in AnyBody Technology A/S. None of the other authors have any financial or personal relationships with other people or organization that could inappropriately influence their work.

Funding

We thankfully acknowledge the financial support by fonds NutsOhra (1302-032).

Ethical approval

Not required.

Acknowledgment

We thank Dominika Ignasiak and Stephen J. Ferguson from Institute for Biomechanics, Switzerland for giving us the opportunity to study their thoracolumbar spine model.

References

[1] Nachemson A, Elfstrom G. Intravital dynamic pressure measurements in lumbar discs. Scand J Rehabil Med 1970;2(suppl 1):1–40.
[2] Schultz A, Andersson G, Ortengren R, Haderspeck K, Nachemson A. Loads on the lumbar spine. validation of a biomechanical analysis by measurements of intradiscal pressures and myoelectric signals. J Bone Joint Surg Am 1982;64(5):713–20.
[3] Sato K, Kikuchi S, Yonezawa T. In vivo intradiscal pressure measurement in healthy individuals and in patients with ongoing back problems. Spine 1999;24(23):2468.
[4] Wilke H-J, Neef P, Hinz B, Seidel H, Claes L. Intradiscal pressure together with anthropometric data–a data set for the validation of models. Clin Biomech 2001;16:S111–26.
[5] Takahashi I, Kikuchi S-i, Sato K, Sato N. Mechanical load of the lumbar spine during forward bending motion of the trunk–a biomechanical study. Spine 2006;31(1):18–23.
[6] Polga DJ, Beaubien BP, Kallemeier PM, Schellhas KP, Lew WD, Buttermann GR, et al. Measurement of in vivo intradiscal pressure in healthy thoracic intervertebral discs. Spine 2004;29(12):1320–4.
[7] Rohlmann A, Graichen F, Kayser R, Bender A, Bergmann G. Loads on a telemeterized vertebral body replacement measured in two patients. Spine 2008;33(11):1170–9.
[8] De Zee M, Hansen L, Wong C, Rasmussen J, Simonsen EB. A generic detailed rigid-body lumbar spine model. J Biomech 2007;40(6):1219–27.
[9] Christophy M, Senan NAF, Lotz JC, O'Reilly OM. A musculoskeletal model for the lumbar spine. Biomech Model Mechanobiol 2012;11(1-2):19–34.
[10] Gagnon D, Arjmand N, Plamondon A, Shirazi-Adl A, Larivière C. An improved multi-joint EMG-assisted optimization approach to estimate joint and muscle forces in a musculoskeletal model of the lumbar spine. J Biomech 2011;44(8):1521–9.
[11] Ghezelbash F, El Ouaaid Z, Shirazi-Adl A, Plamondon A, Arjmand N. Trunk musculoskeletal response in maximum voluntary exertions: a combined measurement-modeling investigation. J Biomech 2018;70:124–33.
[12] Bruno AG, Bouxsein ML, Anderson DE. Development and validation of a musculoskeletal model of the fully articulated thoracolumbar spine and rib cage. J Biomech Eng 2015;137(8):081003.
[13] Ignasiak D, Dendorfer S, Ferguson SJ. Thoracolumbar spine model with articulated ribcage for the prediction of dynamic spinal loading. J Biomech 2016;49(6):959–66.
[14] Khurelbaatar T, Kim K, Kim YH. A Cervico-Thoraco-Lumbar multibody dynamic model for the estimation of joint loads and muscle forces. J Biomech Eng 2015;137(11):111001.
[15] Borst J, Forbes PA, Happee R, Veeger DH. Muscle parameters for musculoskeletal modelling of the human neck. Clin Biomech 2011;26(4):343–51.
[16] Ignasiak D, Ferguson SJ, Arjmand N. A rigid thorax assumption affects model loading predictions at the upper but not lower lumbar levels. J Biomech 2016;49(13):3074–8.
[17] Delp SL, Suryanarayanan S, Murray WM, Uhlir J, Triolo RJ. Architecture of the rectus abdominis, quadratus lumborum, and erector spinae. J Biomech 2001;34(3):371–5.
[18] Carbone V, van der Krogt M, Koopman HF, Verdonschot N. Sensitivity of subject-specific models to hill muscle–tendon model parameters in simulations of gait. J Biomech 2016;49(9):1953–60.
[19] Brown SH, Gerling ME. Importance of sarcomere length when determining muscle physiological cross-sectional area: a spine example. Proc Inst Mech Eng Part H J Eng Med 2012;226(5):384–8.
[20] Bayoglu R, Geeraedts L, Groenen KH, Verdonschot N, Koopman B, Homminga J. Twente spine model: a complete and coherent dataset for musculo-skeletal modeling of the lumbar region of the human spine. J Biomech 2017;53:111–19.
[21] Bayoglu R, Geeraedts L, Groenen KH, Verdonschot N, Koopman B, Homminga J. Twente spine model: a complete and coherent dataset for musculo-skeletal modeling of the thoracic and cervical regions of the human spine. J Biomech 2017;58:52–63.
[22] Pearsall DJ, Reid JG, Livingston LA. Segmental inertial parameters of the human trunk as determined from computed tomography. Ann Biomed Eng 1996;24(2):198–210.
[23] de Jager MKJ. Mathematical head-neck models for acceleration impacts. Copy-Print; 2000.
[24] De Leva P. Adjustments to Zatsiorsky-Seluyanov's segment inertia parameters. J Biomech 1996;29(9):1223–30.
[25] Arjmand N, Gagnon D, Plamondon A, Shirazi-Adl A, Lariviere C. A comparative study of two trunk biomechanical models under symmetric and asymmetric loadings. J Biomech 2010;43(3):485–91.
[26] Stokes IA. Three-dimensional terminology of spinal deformity: a report presented to the scoliosis research society by the scoliosis research society working group on 3-d terminology of spinal deformity.. Spine 1994;19(2):236–48.
[27] Rasmussen J, Damsgaard M, Voigt M. Muscle recruitment by the min/max criterion - a comparative numerical study. J Biomech 2001;34(3):409–15.
[28] Pearcy MJ, Bogduk N. Instantaneous axes of rotation of the lumbar intervertebral joints.. Spine 1988;13(9):1033–41.
[29] Dvorak J, Panjabi M, Novotny J, Antinnes J. In vivo flexion/extension of the normal cervical spine. J Orthop Res 1991;9(6):828–34.
[30] Minotti P, Lexcellent C. Geometric and kinematic modelling of a human costal slice. J Biomech 1991;24(3-4):213–21.
[31] Schultz A, Belytschko T, Andriacchi T, Galante J. Analog studies of forces in the human spine: mechanical properties and motion segment behavior. J Biomech 1973;6(4):373–83.
[32] Schultz AB, Benson DR, Hirsch C. Force-deformation properties of human costo-sternal and costo-vertebral articulations. J Biomech 1974;7(3):311IN23313–227318.
[33] Duprey S, Subit D, Guillemot H, Kent RW. Biomechanical properties of the costovertebral joint. Med Eng Phys 2010;32(2):222–7.
[34] Andersen MS, Damsgaard M, Rasmussen J. Kinematic analysis of over-determinate biomechanical systems. Comput Methods Biomech Biomed Eng 2009;12(4):371–84.
[35] Dreischarf M, Rohlmann A, Zhu R, Schmidt H, Zander T. Is it possible to estimate the compressive force in the lumbar spine from intradiscal pressure measurements? A finite element evaluation. Med Eng Phys 2013;35(9):1385–90.
[36] Dreischarf M, Shirazi-Adl A, Arjmand N, Rohlmann A, Schmidt H. Estimation of loads on human lumbar spine: a review of in vivo and computational model studies. J Biomech 2016;49(6):833–45.
[37] White I, Panjabi AAM. The basic kinematics of the human spine: a review of past and current knowledge.. Spine 1978;3(1):12–20.
[38] Wong KW, Luk KD, Leong JC, Wong SF, Wong KK. Continuous dynamic spinal motion analysis. Spine 2006;31(4):414–19.
[39] Fujii R, Sakaura H, Mukai Y, Hosono N, Ishii T, Iwasaki M, et al. Kinematics of the lumbar spine in trunk rotation: in vivo three-dimensional analysis using magnetic resonance imaging. Eur Spine J 2007;16(11):1867–74.
[40] Rozumalski A, Schwartz MH, Wervey R, Swanson A, Dykes DC, Novacheck T. The in vivo three-dimensional motion of the human lumbar spine during gait. Gait Posture 2008;28(3):378–84.
[41] Fujimori T, Iwasaki M, Nagamoto Y, Ishii T, Kashii M, Murase T, et al. Kinematics of the thoracic spine in trunk rotation: in vivo 3-dimensional analysis. Spine 2012;37(21):E1318–28.
[42] Fujimori T, Iwasaki M, Nagamoto Y, Matsuo Y, Ishii T, Sugiura T, et al. Kinematics of the thoracic spine in trunk lateral bending: in vivo three-dimensional analysis. Spine J 2014;14(9):1991–9.
[43] Tafazzol A, Arjmand N, Shirazi-Adl A, Parnianpour M. Lumbopelvic rhythm during forward and backward sagittal trunk rotations: combined in vivo measurement with inertial tracking device and biomechanical modeling. Clin Biomech 2014;29(1):7–13.
[44] Han K-S, Zander T, Taylor WR, Rohlmann A. An enhanced and validated generic thoraco-lumbar spine model for prediction of muscle forces. Med Eng Phys 2012;34(6):709–16.
[45] Homminga J, Lehr AM, Meijer GJ, Janssen MM, Schlösser TP, Verkerke GJ, et al. Posteriorly directed shear loads and disc degeneration affect the torsional stiffness of spinal motion segments: a biomechanical modeling study. Spine 2013;38(21):E1313–19.
[46] Briggs AM, Van Dieën JH, Wrigley TV, Greig AM, Phillips B, Lo SK, et al. Thoracic kyphosis affects spinal loads and trunk muscle force. Phys Ther 2007;87(5):595–607.
[47] Iyer S, Christiansen BA, Roberts BJ, Valentine MJ, Manoharan RK, Bouxsein ML. A biomechanical model for estimating loads on thoracic and lumbar vertebrae. Clin Biomech 2010;25(9):853–8.
[48] Panjabi MM, Takata K, Goel V, Federico D, Oxland T, Duranceau J, et al. Thoracic human vertebrae quantitative three-dimensional anatomy. Spine 1991;16(8):888–901.
[49] Snijders CJ, Van Dijke GH, Roosch E. A biomechanical model for the analysis of the cervical spine in static postures. Journal of Biomechanics 1991;24(9):783–92.
[50] Meng X, Bruno AG, Cheng B, Wang W, Bouxsein ML, Anderson DE. Incorporating six degree-of-freedom intervertebral joint stiffness in a lumbar spine musculoskeletal model - method and performance in flexed postures. J Biomech Eng 2015;137(10):101008.
[51] Senteler M, Aiyangar A, Weisse B, Farshad M, Snedeker JG. Sensitivity of intervertebral joint forces to center of rotation location and trends along its migration path. J Biomech 2018;70:140–8.
[52] Ghezelbash F, Eskandari A, Shirazi-Adl A, Arjmand N, El-Ouaaid Z, Plamondon A. Effects of motion segment simulation and joint positioning on spinal loads in trunk musculoskeletal models. J Biomech 2018;70:149–56.
[53] Ashton-Miller JA, Schultz AB. Biomechanics of the human spine and trunk. Exerc Sport Sci Rev 1988;16(1):169–204.
[54] Andriacchi T, Schultz A, Belytschko T, Galante J. A model for studies of mechanical interactions between the human spine and rib cage. J Biomech 1974;7(6):497–507.